Line emission from hot, dense, aluminum plasmas

D. Duston* and J. Davis
Plasma Radiation Group, Naval Research Laboratory, Washington, D. C. 20375
(Received 30 July 1979)

The radiation emission from dense, high-temperature aluminum plasmas has been studied to appraise the influence of photoexcitation on several spectral diagnostics currently used to determine average plasma parameters. The plasma state is described by a set of collisional-radiative rate equations characterizing the competing atomic processes occurring in a homogeneous plasma volume of constant density and temperature. Radiation is transported through the plasma by the method of frequency diffusion, a technique which employs collision times of the photons as they diffuse through the wings of a broadened line profile. Line spectra and line-intensity ratios for several pairs of emission lines of the K shell are calculated in optically dense plasmas and compared with those obtained from the model within the optically thin approximation. The radiation-trapping effects are shown significantly to modify the behavior of the optically thin constant-density or constant-temperature line ratio curves, which become double valued in some cases. Comparisons of state populations obtained from this model and the local-thermodynamic-equilibrium model are also shown.

I. INTRODUCTION

It has been suggested from recent experiments[1,2] in which moderate-Z plasmas have been heated to high temperatures at high density, that the resulting radiation emission may play in important role in the dynamic evolution of the plasma temperature and density profile. The extent to which the radiation may represent a significant energy-loss mechanism is a moot question,[3] but clearly, resonance reabsorption of emitted photons in an optically thick medium will both redistribute the plasma energy, spatially and spectrally,[4] and can alter significantly the radiation signature at the diagnostic detectors.

In an effort to provide theoretical insight into some of the effects of radiation and ionization on the plasma development, several atomic models have recently been developed[5-9] which take into account the various processes occurring in high-temperature plasmas and which ultimately affect the radiation emission. While a complete theoretical analysis of the radiation dynamics and its interplay with other basic plasma processes requires a full-scale, detailed, time-dependent model coupling ionization dynamics with magnetohydrodynamics, we feel that the atomic processes leading to the radiation emission are sufficiently complex that a better understanding of the radiation physics would be more realizable if the model were limited, initially, to the basic ionization and radiation processes, in the absence of convection.

In this work, we present results from our radiation-ionization model as applied to the problem of diagnostics in a dense high-temperature aluminum plasma, with the notion that systematic trends in the emission features calculated from this model will lead to conclusions about the nature of the radiating plasma. These results will be compared with those obtained from different physical models as well as with other investigations.[9-11]

II. MODEL PREDICTIONS

The ionization-dynamic model employed in this study is similar to our earlier model.[8,12,13] A general set of time-dependent atomic rate equations are solved for a stationary volume element of plasma, homogeneous in temperature and total ion density. Each equation describes the population and depopulation of a particular ion (atom) species as determined by rate coefficients characterizing the various collisional events the particles experience. Such an equation, in the absence of convection, would be

$$\frac{dN_i}{dt} = \sum_j W_{ji} N_j - \sum_j W_{ij} N_i \,, \tag{1}$$

where W_{ij} is the rate describing a transition from state i to j (in $\sec^{-1}$). Each ground state and excited level in the model is represented by an equation of the form given by (1). The collisional and radiative processes are described by the rate W_{ij}. The model currently includes the following atomic processes: Collisional ionization, collisional (3-body), radiative (2-body), and dielectronic recombination, collisional excitation, collisional and spontaneous radiative de-excitation. The collisional ionization rates were calculated using a prescription suggested by Seaton,[14] and the radiative recombination rate coefficients were calculated by the detailed balance of photoioniza-

tion rates[15] employing effective Gaunt factors.[16] The dielectronic recombination rate coefficients are those calculated by Jacobs *et al.*,[17] while the spontaneous decay rates were taken from the NBS tables[18] or from oscillator strength extrapolations.[13] The electron collisional-excitation rate coefficients were calculated in the Born approximation[19] for the hydrogenlike transitions and by the distorted-wave method[20] for the heliumlike and lithiumlike transitions. The rates for the collisional processes from higher to lower energy states were calculated by the detailed balance of the corresponding upward collisional rate coefficients.

The processes of photoexcitation and stimulated emission are taken into account by a phenomenological transport model which allows photons to escape from an optically thick plasma by scattering into the optically thin wings of the absorption line profile. The photon-loss rate depends upon the optical depth of the plasma,

$$\tau_\nu = \frac{\pi e^2}{m_e c} f_{ij} \frac{\bar{L} N_i}{\sqrt{\pi}\Delta\nu_D} \varphi(\nu), \tag{2}$$

where f is the line oscillator strength, N_i is the lower-state density, and φ is the line-profile function; the Doppler width is given by

$$\Delta\nu_D = (2T_i/Mc^2)^{1/2}\nu_0, \tag{3}$$

where T_i is the ion temperature, M is the ion mass, and ν_0 is the line-center frequency. The effective photon path length across the plasma is given by $\bar{L}$; in this way an average measure of the spatial extent of the optically thick plasma is taken into account. We can write an equation for the collisional processes undergone by photons in going from state j to state i, viz.,

$$\frac{dN_{ji}^p}{dt} = N_j A_{ji} + \frac{1}{t_s} N_{ji}^p \frac{g_i N_j}{g_j N_i} - \left(\frac{1}{t_s} + \frac{1}{t_e}\right) N_{ji}^p, \tag{4}$$

where A is the Einstein coefficient, N^p is the photon density, and t_s and t_e are scattering and escape times for the photon, respectively. The terms on the right-hand side of (4) describe spontaneous decay, stimulated emission, stimulated absorption and escape. We can rewrite Eq. (1) to include the photon transport terms,

$$\frac{dN_j}{dt} = \sum_k W_{kj} N_k - \sum_k W_{jk} N_j + \sum_{i<j} \left(\frac{1}{t_s} N_{ji}^p - \frac{1}{t_s}\frac{g_i N_j}{g_j N_i} N_{ji}^p\right). \tag{5}$$

Assuming that the photon processes occur on a time scale faster than the other collisional processes, the time derivative is set to zero in (4), N^p is solved for and substituted into (5), removing the A_{ji} term from W_{jk}. This yields the probability that a photon born at plasma center will escape to the outside (NA times probability); an integration over r is then performed to average over all photons born throughout the plasma volume (with $\bar{L}$ replaced by r in the optical depth) to obtain

$$\gamma = \frac{1}{R}\int_0^R \left[1 + \frac{t_e}{t_s}\left(1 - \frac{g_i N_j}{g_j N_i}\right)\right]^{-1} dr. \tag{6}$$

We incorporate this factor in the rate equations *and* in the radiation calculation,

$$P_\nu = h\nu N_{ji} A_{ji} \gamma. \tag{7}$$

Hence, both the attenuation of the radiation by opacity and the optical pumping effects on the level populations are included self-consistently. To evaluate γ, expressions for t_e and t_s have been derived as a function of the broadening mechanism influencing the line profile. For a naturally broadened line, the plasma is assumed to be optically thin, $\tau < 1$, and $t_e = 0$. For Doppler and Voigt line profiles, respectively the expressions can be used for t_e/t_s,[13,21,22]

$$t_e/t_s = \begin{cases} \tau_0(\pi \ln\tau_0)^{1/2}(1 + 1/2\ln\tau_0) \\ 3(\tau_0/a)^{1/2} - 1, \end{cases} \tag{8}$$

where τ_0 is the optical depth at line center ($\nu = \nu_0$) and a is a damping parameter given by

$$a_{ji} = \frac{\sum_k (A_{jk} + C_{jk}) + \sum_k (A_{ik} + C_{ik})}{4\pi\Delta\nu_D}, \tag{9}$$

with C representing collisional rates. Hence, the Voigt profile is broadened by both collisional and radiative processes from emitting and absorbing states.

Preliminary studies of the radiation emission using these two broadening mechanisms indicate that under most plasma conditions, a Doppler line profile will result in more attenuation of line radiation than will a Voigt profile, primarily because photons can escape in the extended wing structure of the Voigt profile.

In order to test its validity, this method of radiation transport has been applied to a two-level atom for an infinite slab plasma medium[23] and the fluxes and radiation field departure coefficients compare quite favorably with Hearn's numerical solution of the exact radiation transport equation in this geometry.[24]

Aluminum was selected for study because of our

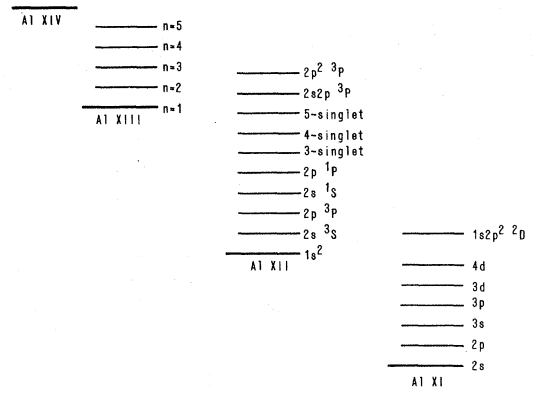

FIG. 1. Aluminum level structure used in the CRE model.

previous experience and understanding of aluminum models and the availability of experimental results.[25-27] Basic to any theoretical calculation of this kind is the atomic level structure; for aluminum we have included the 14 ground states, 4 excited levels in Al XIII ($n=2,3,4,5$), 7 levels in Al XII ($2s\,^3S$, $2p\,^3P$, $2s\,^1S$, $2p\,^1P$, 3-singlet, 4-singlet, and 5-singlet), and 5 levels in Al XI ($2p$, $3s$, $3p$, $3d$, $4d$). In addition, we include 3 double-excited levels ($2s2p\,^3P$, $2p^2\,^3P$, $1s2p^2\,^2D$) in order to study some prominent satellite lines in the spectra of high-temperature aluminum plasmas; the level structure is depicted in Fig. 1. Note that we have represented individual nl components of the hydrogenlike ion and the higher Rydberg levels of the heliumlike ion as single degenerate n states. The collisional rates by both ions and electrons which couple the $\Delta n=0$ transitions for these levels have been assessed in a previous work[13] and have been found to be sufficiently large over a wide range of densities and temperatures that the various l states are populated according to their relative statistical weights. Hence, for all Al XIII states and for $n\geq 3$ in Al XII, we have previously averaged the rates which describe processes initiating or terminating on an individual nl level over all possible values of l for a given n, according to the statistical weights. Thus, the collisional-excitation rate from the $1s^2$ state to the n=3 singlet level, for example, is obtained from the individual rates coupling the $1s^2$ state to the $3s$, $3p$, and $3d$ singlet levels.

III. RESULTS

A. Line spectrum from aluminum plasmas

One reason for performing calculations of this type is to predict level populations and radiation emission from a plasma characterized by electron temperature, ion density, and size. As an example of the information obtained from our collisional-radiative equilibrium (CRE) model about state-density populations, an abundance curve showing the distribution of ionization-state populations as a function of temperature at a constant ion density of 10^{20} cm^{-3} in the optically thin approximation is shown in Fig. 2. The higher peaks corresponding to Al IV and Al XII are due to the large ionization energy of a closed-shell configuration. These peaks are usually broader in temperature indicating the propensity of the atom to remain in such a configuration. In Fig. 3, the "thin" abundances of Al XI–Al XIV are shown as a function of ion density for an electron temperature of 300 eV. Note that over a wide range of densities, the closed-shell Al XII ion is again the dominant species.

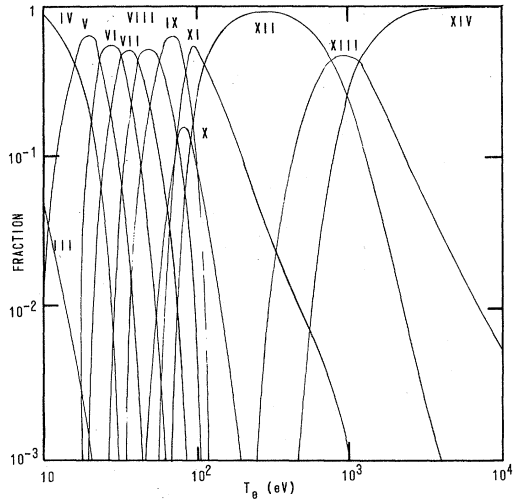

FIG. 2. Aluminum abundance curves vs electron temperature for an ion density of 10^{20} cm^{-3} (optically thin).

A typical x-ray spectrum as calculated by our

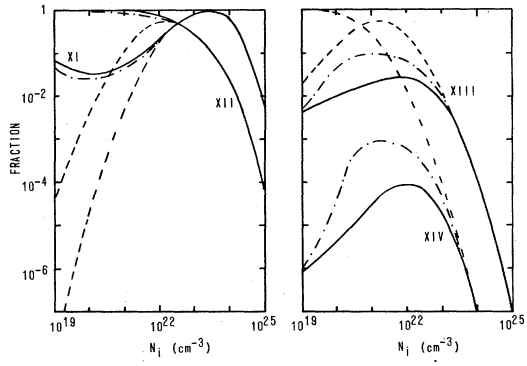

FIG. 3. Aluminum abundance curves vs ion density for an electron temperature of 300 eV: CRE-thin (–), CRE-thick (– ·–), LTE (– – –).

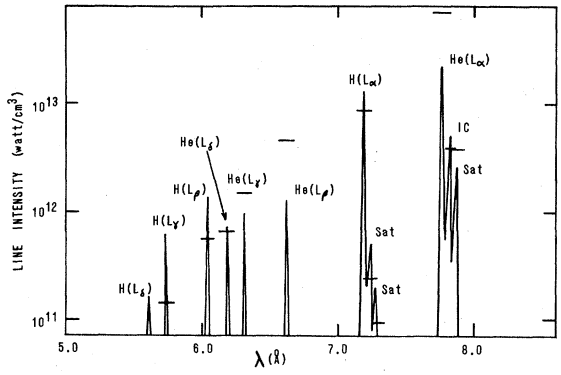

FIG. 4. Aluminum line emission spectrum, 5–8 Å, for an ion density of 10^{20} cm^{-3}, electron temperature of 500 eV and radius of 100 μm.

model is shown in Fig. 4 and the corresponding vacuum ultraviolet (vuv) spectrum in Fig. 5, for a plasma at 300 eV, a density of 10^{20} ions/cm^3 and a radius of 100 μm for a Voigt profile. All lines in Fig. 4 decay to the $1s$ or $1s^2$ ground-state levels, whereas, in Fig. 5, all transitions terminate on an $n=2$ level. The Al XII Balmer series lines, e.g., He $(2p\,^1P\text{-}3^1)$, are actually a manifold of the p-s and p-d transitions, but since levels with principle quantum number greater than 2 are considered as degenerate in our model, only their combined intensities are shown in Fig. 5. Also notice the satellite structure to the long-wavelength side of the hydrogenlike and heliumlike resonance lines; these satellites are due to the transitions $1s2s\,^3S\text{-}2s2p\,^3P$, $1s2p\,^3P\text{-}2p^2\,^3P$, and $1s^22p\,^2P\text{-}1s2p^2\,^2D$, and are important both as relatively strong emitters and as valuable plasma diagnostics.

In order to illustrate the significance of photoexcitation on the radiation emission of dense plasmas, we have indicated the line intensities for a plasma with identical equilibrium conditions, but

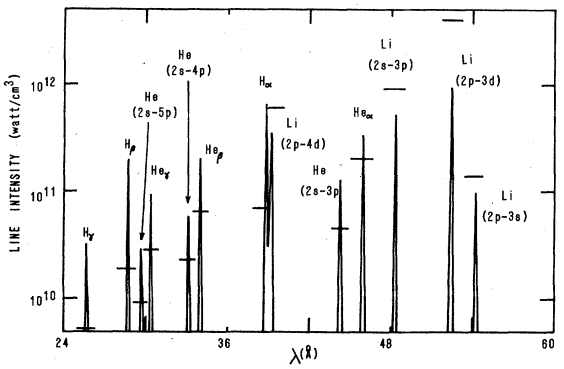

FIG. 5. Aluminum line emission spectrum 24–60 Å for an ion density of 10^{20} cm^{-3}, electron temperature of 500 eV and radius of 100 μm.

calculated in the optically thin approximation by horizontal lines through the intensity spikes in Figs. 4 and 5. The differences are seen to range from a few percent, as in the case of the intercombination (IC) line, to more than an order of magnitude as with the H_β line. In general, one would expect lines with large optical depths to experience a decrease in intensity due to the large photoexcitation cross section. This is , in fact, the case for the heliumlike Lyman lines and lithiumlike lines shown in the spectra, including the He(L_α) satellite line. The intercombination transition is unaffected because, in spite of the fact that its lower level is a highly populated ground state, it has a rather small spontaneous decay coefficient $(2.5\times10^{10}\ \text{sec}^{-1})$, and hence, a relatively small optical depth ($\tau_0=0.23$) compared to that of the heliumlike resonance line ($\tau_0=83$).

The hydrogenlike and heliumlike Balmer-series lines show a universal increase in intensity when radiation trapping is included in the calculation. Since their lower states are excited states of the ions ($n=2$ levels), their optical depths are small, and little photon reabsorption takes place. In addition, the Lyman-series lines are so optically thick that the power levels are "optically pumped" by the stimulated absorption process and the net effect of the increase in upper-state populations is a corresponding increase in intensities of the optically thin Balmer-series lines when opacity is included. Note, however, the He(L_6) line; although it is a Lyman-series transition, and has an optical depth of about 2.4, the increase in the $5p$ population due to pumping more than compensates for the attenuation of the line intensity by photoabsorption.

An apparent contradiction to the above argument concerning lines with large optical depth is seen to occur in Fig. 4, where it is shown that the hydrogenlike Lyman-series lines are universally stronger in the thick calculation than in the thin, even though the optical depths of the α, β, and γ lines are 28.7, 4.6, and 1.6, respectively. In fact, these lines are somewhat attenuated by photoabsorption, but an actual *increase* in the thick intensities is caused by a significant enhancement of the Al XIII ground state by collisional ionization from the Al XII excited states, whose populations are now optically pumped. In order to verify this effect, a calculation was performed in which the radiation transport was "turned off" in the hydrogenlike ion. The intensity of the H(L_α) line was then calculated to be over 2×10^{13} W/cm^3, thus indicating that the states of Al XIII receive an increase in population from Al XII states in the optically thick case which exceeds the decrease in line intensity from the hydrogenlike Lyman lines

due to photon absorption. Hence, we have a case where it is possible that an optically thick transition may radiate at a *higher* intensity than would be calculated in an optically thin approximation, due to the strong collisional coupling between ions and significant optical pumping.

B. Diagnostic line ratios in the optically thin approximation

Spectral line intensity ratios are a valuable diagnostic tool employed by spectroscopists to determine the average temperature and density of the emitting region of a plasma. Although absolute line intensities are directly linked to the radiation source function, they are difficult measurements to make, requiring extremely accurate calibration of the detector. Taking the ratio of two emission lines eliminates some of the more difficult aspects of this calibration; in addition, if the two lines lie in the same region of the spectrum, technical problems due to nonlinearity of film or crystal response are lessened. We have chosen to study the behavior of five line ratios commonly used in the plasma community to diagnose laboratory and astrophysical plasma sources. The ratio of the hydrogenlike resonance line ($1s$-$2p$) to the heliumlike resonance line ($1s^2$-$1s2p$ ^1P) and the lithiumlike satellite line ($1s^22p$-$1s2p^2$ ^2D) to the heliumlike resonance line are both used to determine electron temperature. Similarly, the ratio of the hydrogenlike resonance line to the heliumlike L_β line ($1s^2$-$1s3p$ ^1P) and the hydrogenlike L_β ($1s$-$3p$) to the heliumlike L_δ ($1s^2$-$1s5p$ ^1P) are temperature diagnostic ratios. Finally, the ratio of the heliumlike intercombination (IC) line ($1s^2$-$1s2p$ ^3P) to the heliumlike L_α is used to determine density.

In general, a good temperature diagnostic ratio is relatively insensitive to changes in density while the converse is true for a good density diagnostic ratio. We have plotted the density dependence of several of the ratios against ion density from calculations done with the CRE model (as shown in Figs. 6–10); these calculations have been done assuming an optically thin plasma, temporarily neglecting reabsorption, in order to see the effects of particle collisions on the ratios as the plasma goes from a coronal to a collisional regime. The Al XI satellite to Al XII L_α ratio in Fig. 6 is relatively flat up to a density of 10^{21} for the temperatures displayed. Above this density, the ratio increases due to a combination of two effects: The increasing ratio of Al XII ground-state population to Al XIII ground-state population and the strong collisional coupling between the Al XIII ground state and the $1s2p$ ^1P level. At low densities, both the $1s2p$ Al XII state and the $1s2p^2$ ^2D Al XI state are strongly coupled to the Al XII ground state by electron collisions; consequently the ratio is nearly constant with density. As the density increases, the collisional recombination from the Al XIII ground state becomes the dominant mechanism populating the $1s2p$ level, uncoupling this level to some degree from the Al XII ground state. At the same time, the fractional population of the Al XIII ground state decreases more rapidly with density than the Al XII ground state (see Fig. 3). This leads to a relative in-

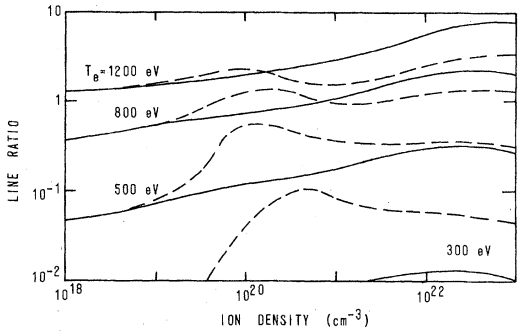

FIG. 7. $1s$-$2p$/$1s^2$-$1s2p$ (^1P) line ratio vs ion density; optically thin (–), optically thick with radius of 100 μm (---).

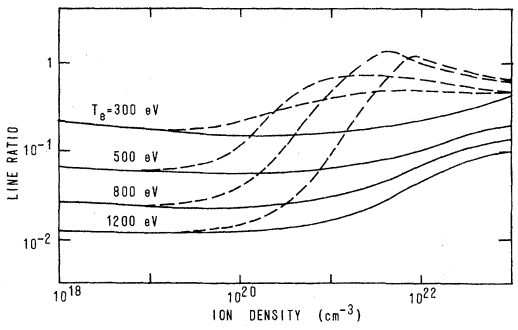

FIG. 6. $1s^2 2p$ (^2P)-$1s2p^2$ (^2D)/$1s^2$-$1s2p$ (^1P) line ratio vs ion density; optically thin (–), optically thick with radius of 100 μm (---).

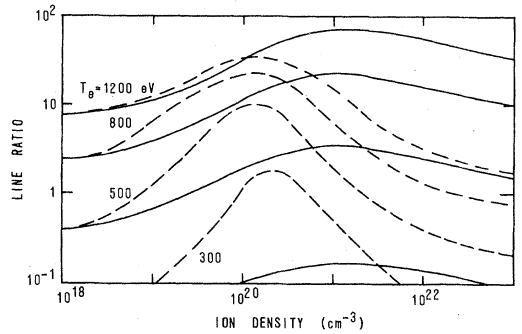

FIG. 8. $1s$-$2p$/$1s^2$-$1s3p$ (^1P) line ratio vs ion density; optically thin (–), optically thick with radius of 100 μm (---).

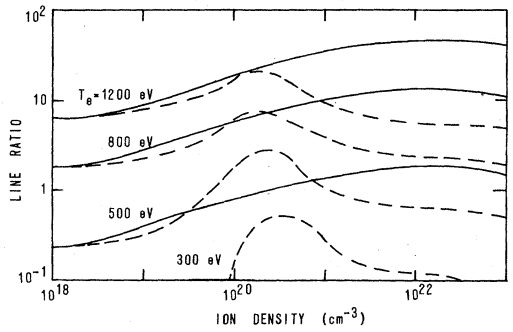

FIG. 9. $1s$-$3p/1s^2$-$1s5p(^1P)$ line ratio vs ion density; optically thin (-), optically thick with radius of 100 μm (---).

crease in the ratio of the $1s2p^2$ to $1s2p$ populations and a corresponding increase in the line intensity ratio. Notice that the increase occurs at a slightly lower density for the higher temperature curves. This is due to the greater fractional population of the hydrogenlike ground state at higher temperatures; this enhances the coupling of the $1s2p\,^1P$ state to this ground state making its population less strongly coupled to the heliumlike ground state, yielding the density-sensitive result the ratio displays at higher ion densities.

The hydrogenlike L_α to heliumlike L_α ratio in Fig. 7, the hydrogenlike L_α to heliumlike L_β ratio in Fig. 8, and the hydrogenlike L_β to heliumlike L_6 ratio in Fig. 9 all display a definite density effect at the temperatures studied. As seen from Fig. 3, the distribution of the heliumlike ground state is flat at low densities and drops off at higher densities; the hydrogenlike ground state is more peaked with a maximum near 10^{22} ions/cm^3. The line ratios in Figs. 7, 8, and 9 reflect these distributions rather plainly, with definite maxima occurring in the 10^{21}–10^{23} ions/cm^3 range. It is interesting to note that while these ratios possess

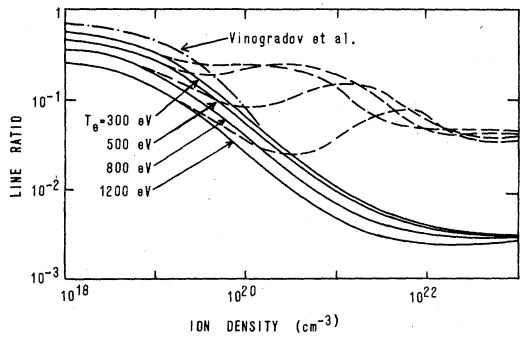

FIG. 10. $1s^2$-$1s2p(^3P)/1s^2$-$1s2p(^1P)$ line ratio vs ion density; optically thin (-), optically thick with radius of 100 μm (---).

this undesirable density dependence, a knowledge of the density to within an order of magnitude allows one to predict an electron temperature from the curves with an uncertainty of usually less than 100 eV. Since most experimental plasmas are able to be diagnosed easily to densities within this range, these line ratios are still valuable indications of the plasma temperature.

The intercombination-to-resonance line ratio in Fig. 10 is a well-known density diagnostic[28] used with reasonable success[29,30] for laboratory plasma. The intercombination line is usually a very weak line compared to the heliumlike resonance line due to a relatively small radiative decay rate. As Z increases, however, this coefficient increases to within less than a few orders of magnitude of the decay rate of the resonance line, and a reasonable line ratio measurement can usually be made for $Z \geq 11$. At low densities, both the $1s2p\,^1P$ and $1s2p\,^3P$ levels are populated by electron collisions from the ground state and depopulated by spontaneous decay, yielding a rather constant ratio at corona densities. As the density increases, however, collisional effects coupling the four $n=2$ levels become increasingly important. The effect is twofold: The density of the rapidly decaying singlet P level is increased from contributions from the other states, while the highly populated slowly decaying, triplet P level suffers depopulation through contributions to other $n=2$ states. The ratio thus drops rapidly until a density is achieved at which the local-thermodynamic-equilibrium (LTE) state distributions are reached and the ratio becomes constant again. This value is given simply by

$$R = \frac{(gA)\,(\text{triplet})}{(gA)\,(\text{singlet})}. \tag{10}$$

Using statistical weights and Einstein coefficients of 9 and 2.54×10^{10} sec^{-1} for the ^3P level, and 3 and 2.83×10^{13} sec^{-1} for the ^1P level gives us a value for R of 2.69×10^{-3}, in excellent agreement with Fig. 10 at 10^{23} ions/cm^2. Although the curves display some temperature dependence, an uncertainty of 300 eV in electron temperature will result in, at most, an error in the density determination of less than a factor of 2, reasonably good accuracy for this plasma parameter. Also plotted in Fig. 10 is the intercombination-to-resonance line ratio as calculated by Vinogradov *et al.*[28] for an aluminum plasma at an electron temperature of 360 eV. Although the ratio is only given up to an ion density of 10^{20} cm^{-3} in that study, the agreement between the two calculations is very good. The small differences between the values obtained from that work and ours are attributed to the fact that the collisional-excitation and col-

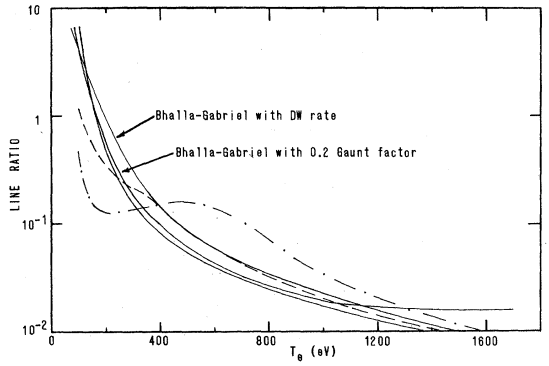

FIG. 11. $1s^2 2p(^2P)$-$1s2p^2(^2D)/1s^2$-$1s2p(^1P)$ line ratio vs electron temperature; optically thin (-), optically thick for 50-μm (---) and 500-μm (-·-) plasma.

lisional-ionization-rate coefficients used in the two studies have been calculated by different methods.[13] In addition, the radiative decay rate used in that work for the $1s2p(^3P)$-$1s^2$ transition differs slightly from the one used in our model.[31] However, the similarities between the predictions of the two models is encouraging.

The temperature dependence of the four temperature-sensitive ratios have been plotted in Figs. 11–14 for an optically thin plasma (solid lines) at a density of 10^{20} ions/cm^3. The satellite-to-resonance line ratio in Fig. 11 displays the usual $T_e^{-1}e^{-E/T_e}$ behavior resulting from an analysis of the $1s^2$, $1s2p\,^1P$, $1s2p^2\,^2D$ 3-level system. Balancing the population of the doubly excited lithiumlike state by electron capture with the depopulation of this state by autoionization and spontaneous radiative decay yields the dielectronic recombination (DR) rate[32]

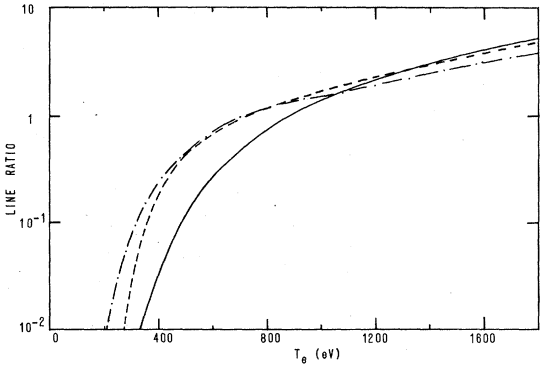

FIG. 12. $1s$-$2p/1s^2$-$1s2p(^1P)$ line ratio vs electron temperature; optically thin (-), optically thick for 50-μm (---) and 500-μm (-·-) plasma.

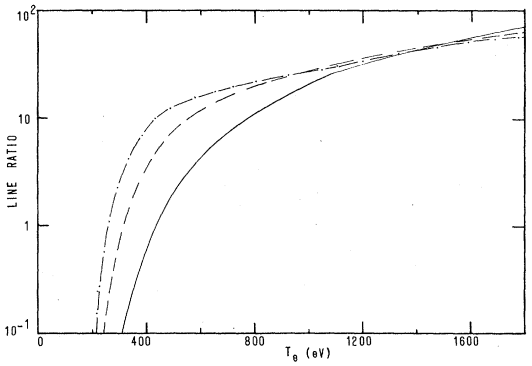

FIG. 13. $1s$-$2p/1s^2$-$1s3p(^1P)$ line ratio vs electron temperature; optically thin (-), optically thick for 50-μm (---) and 500-μm (-·-) plasma.

$$\alpha_{\mathrm{DR}} = 2.06\times10^{-16}\frac{g_s}{g_g}A_r \times\left(\frac{A_a}{A_a+A_r}\right)T_e^{-3/2}e^{-E_s/T_e}, \tag{11}$$

where g_s and g_g are statistical weights of the doubly excited and heliumlike ground states, A_r and A_a are the radiative decay and autoionization rates for the doubly excited state, and E_s is the energy separation between the $1s^2$ and $1s2p^2\,^2D$ states. A value for the line ratio can be obtained by dividing α_{DR} by the electron collisional-excitation rate from the $1s^2$ to the $1s2p\,^1P$ level. An approximate expression for this rate due to Van Regemorter[33] is

$$X = 1.7\times10^{-3} f\langle\bar{g}\rangle\Delta E^{-1}T_e^{-1/2}e^{-\Delta E/T_e}, \tag{12}$$

where f is the oscillator strength, $\langle\bar{g}\rangle$ is a thermally averaged Gaunt factor and ΔE is energy separation of the transition. The division of the two rates yields the well-known Bhalla-Gabriel

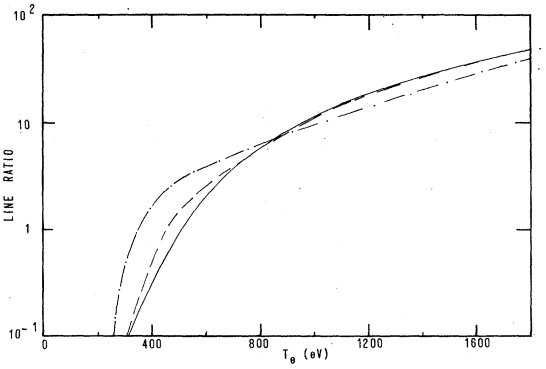

FIG. 14. $1s$-$3p/1s^2$-$1s5p(^1P)$ line ratio vs electron temperature; optically thin (-), optically thick for 50-μm (---) and 500-μm (-·-) plasma.

formula[34] for this line ratio,

$$R = 1.212 \times 10^{-13} \frac{g_s \Delta E}{g_g f \langle \bar{g} \rangle T_e} \times \left(\frac{A_r A_a}{A_r + A_a} \right) e^{(\Delta E - E_s)/T_e}. \quad (13)$$

This result was first derived for use in astrophysical phenomena and has been a valuable diagnostic when the two excited states are populated predominantly from the heliumlike ground state; that is, in low-density regimes. As was stated earlier, at higher densities, the $1s2p\,^1P$ level begins to be affected by contributions from the $1s2s$ ^1S and $1s$ states, and the population density diverges slightly from its coronal value. For comparison, we plotted the analytical result for this ratio alongside the CRE result in Fig. 11. One curve employs a 0.2 value[14] for the Gaunt factor and formula (12) for the excitation rate, while the other uses the distorted-wave result for the excitation rate instead of formula (12) in obtaining the ratio. At an electron temperature of 500 eV, our model predicts the $2s$-$2p$ rate to be 50% of the dominant $1s$-$2p$ rate, even at the nominal density of 10^{20} ions/cm^3 for which Fig. 11 was obtained. The neglect of the complete collisional coupling at these plasma parameters would then result in a predicted radiation intensity from the Al XII L_α line which is 30% lower than the CRE model, a significant error in the emission of the most prominent line in the x-ray region of the aluminum spectra. Hence, when employing this ratio for accurate temperature determination of laboratory plasmas at higher ($>10^{19}$) densities, the analysis requires the complete $n=2$ level system.

The apparent agreement between the curve using the 0.2 Gaunt factor with Eq. (13) and the CRE calculations at lower temperatures is the result of the missing collisional couplings and the inaccurate rate coefficient for the $1s$-$2p$ transition canceling each other in the 0.2 Gaunt factor curve.

The satellite-to-resonance line ratio does present the plasma spectroscopist with some inherent difficulties, however. The sensitivity of the ratio is diminished somewhat at higher temperatures, the resonance line is quick to be affected by opacity, and some experimental difficulties occur when trying to resolve the satellite line completely. On the other hand, the major contribution to both upper levels responsible for this ratio comes from the same level, the heliumlike ground state. When the two upper levels of the ratio originate from separate ion ground states, the danger exists that these ions will appear as strong emitters in different spatial regions of the plasma, and the ratio will yield a meaningless value for the temperature if a temperature gradient exists in the plasma. The validity of these model predictions would then be limited, applying only to experimental spectra which is spatially resolved.

The line ratios in Figs. 12–14 are similar in that they compare a hydrogenlike line intensity with a heliumlike line intensity. The basic feature of all the curves is the monotonic increase in the ratio as the Al XIII ground state becomes more populated, relative to the Al XII ground state. Of the three line ratios, the hydrogenlike L_β to the heliumlike L_6 in Fig. 14 is probably the best one in terms of accuracy. The two transitions which make up the ratio lie at very similar energies (6.055 and 6.18 Å), their spontaneous decay rates are of the same order (4.77×10^{12} and 1.58×10^{12} sec^{-1}), opacity is not expected to affect either line in laboratory-size plasmas until higher densities are achieved, the ratio is of order 1 over a range of electron temperatures (400–800 eV) commonly encountered in laboratory aluminum plasmas, and the sensitivity of the ratio in that range is very good.

C. Line ratios from optically thick plasmas

In order to account for reabsorption of emitted line radiation for optically thick plasmas, we attenuate the escaping photon flux by a phenomenological reduction in the radiative source function. This reduction factor, γ, discussed earlier, is calculated to account for the number of ion scatterings the photon undergoes before it diffuses in frequency to the optically thin wings of the broadened line profile, where it can escape. While this model can accommodate the radiation transfer for a natural, Doppler, or Voigt line profile, the calculations presented here were performed using Voigt line profiles.

We have plotted the line ratio behavior versus density for a plasma with a radius of 100 μm in Figs. 6–10 (broken curves). Comparing these with the optically thin curves, it is found that the thin and thick line ratios are identical at $N_i = 10^{18}$ cm^{-3}, indicating that this plasma is probably transparent to x rays at these densities. Although this is, in fact, the case here, the true indication of whether photon absorption is occurring for a particular line can be found from the optical depth, given by Eq. (2).

An optical depth at line center ($\nu = \nu_0$) of less than 0.1 usually indicates that self-absorption is negligible. However, larger optical depths can occur accompanied by significant photoexcitation in the plasma, yet no effect in the line intensity be apparent. When the plasma is radiation dom-

inated, the rate of stimulated absorption may be quite large due to large τ, but if the downward radiative processes (spontaneous and stimulated) dominate over other collisional processes which destroy the upper state, absorbed photons will be reemitted again and again. This process will continue until the photons redistribute in frequency to the thin wings of the line or in space to the edge of the plasma, where they escape. Hence, an indication of whether photon absorption will affect the line intensity is given by the quenching parameter for a line whose upper state is i and lower state is k,

$$p_q = \frac{\sum_j C_{ij}}{\sum_j C_{ij} + A_{ik}}, \tag{14}$$

where C_{ij} represents collisional rates and A_{ik} is the Einstein coefficient. When p_q is small, collisional quenching of the upper state is not appreciable, and the emitted line intensity will be unaffected by significant reabsorption. A quenching parameter of near one, on the other hand, indicates that any photon reabsorbed is likely to be collisionally quenched, resulting in a large reduction in the line intensity. However, when τ is large, the upper-state population will be altered due to the large photoexcitation rate, regardless of whether p_q is large or small.

Comparing the general features of the curves, all of which include a heliumlike Lyman-series line as part of the line ratio, a common trend is apparent. The curves all display a shoulder structure beginning at densities above 10^{20} ions/cm^3. The onset of this shoulder signals the point at which the Al XII Lyman lines begin to be affected by opacity. The L_α line is usually the first of the lines considered here to be attenuated by reabsorption of photons since its radiative decay rate is the largest and its lower state (which determines the optical depth) is the Al XII ground state, the level which is the most dominant fractional density over a wide range of temperatures and densities. For example, the intercombination line has an Einstein coefficient which is 3 orders of magnitude lower while the satellite line and the Al XIII L_α line are due to transitions which end on different, less populated levels over a significant temperature range. The curves maximize and then turn over as the other line comprising the ratio begins to suffer opacity reduction. In Figs. 6 and 10, where both the upper levels of each ratio are populated predominantly from the $1s^2$ level and general state abundance variations can be folded out, the shoulder appears at a higher density for the high-temperature curves. This is characteristic of the $T^{-1/2}$ dependence of the optical depth [see Eq. (3)]; at high temperatures, the optical depth will become large only at higher densities. Hence, the onset of opacity effects will occur at higher densities for a ratio at 1200 eV than one at 500 eV. In Figs. 7–9, where a hydrogenlike and heliumlike line are compared, the shoulder at 500 eV is larger than the one at 1200 eV, emphasizing the dominance of the Al XII ion at the lower temperature. However, the most striking feature of many of the curves, and, in terms of diagnostics, a rather unfortunate one, is the double-valued nature of the line ratios. This aspect of these curves could render them useless as plasma diagnostics unless either the plasma density is relatively well known or several of the diagnostics are used simultaneously in plasma parameter determinations.

As an analytic check on the model calculations, line-intensity ratios in the LTE (high density) limit *with* opacity effects included have been calculated for the H(L_α) to He(L_α) ratio and the IC to He(L_α) ratio. To first-order approximation with a Voigt profile used in the radiation transport model, the line ratio can be expressed as

$$R = \frac{N_2 A_2 \Delta E_2}{N_1 A_1 \Delta E_1} \left(\frac{\tau_1}{\tau_2}\right)^{1/2}. \tag{15}$$

The main assumption here is that the broadening is nearly the same for the two transitions forming the ratio. The optical depth is proportional to the radiative decay rate, the g factors of upper and lower states, and the lower-state population density; hence Eq. (15) becomes

$$R = \frac{N_2 \Delta E_2}{N_1 \Delta E_1} \left(\frac{A_2 g_2' / g_2 N_1'}{A_1 g_1' / g_1 N_2'}\right)^{1/2}, \tag{16}$$

where the prime refers to the lower state of the transition. In the case of the ratio of the two resonance lines, the Saha equation[10] can be used to calculate the ratio of the $n=2$ and $2p\,^1P$ levels:

$$\frac{N(n=2)}{N(2p^1)} = \frac{2g_{n=2}}{N_e g_{2p}} \left(\frac{m_e k T_e}{2\pi\hbar^2}\right)^{3/2} e^{-\Delta E/kT_e}. \tag{17}$$

A similar expression can be used to get the ratio of the two lower states, the Al XII and Al XIII ground states. Inserting the appropriate atomic parameters, the ratio is calculated to be about 0.26 at 500 eV, which compares quite well with the model prediction of 0.3 in Fig. 7, even though the levels considered here are not in a state of LTE with each other at a density of 10^{23} ions/cm^3. Density criteria for LTE will be discussed in detail in Sec. III D.

The LTE limit for the IC line-to-resonance line ratio is simpler to calculate since (1) the lower state of both transitions is the Al XII ground state and, (2) the strong collisional coupling between

the $2p$ singlet and triplet levels will equilibrate their populations to nearly a 1:3 ratio at even moderate (~10^{23} ions/cm^3) densities. Hence, Eq. (16) becomes (note that the energies are nearly equal),

$$R_{\mathrm{LTE}} \simeq 3\left(\frac{A_{\mathrm{IC}}}{3A_{\mathrm{RES}}}\right)^{1/2}. \tag{18}$$

Inserting the appropriate parameters in (18) yields a value of 0.05 for the LTE ratio of the IC and He(L_α) lines in the optically thick case, while the curves calculated by the model tend to center around 0.04, again, quite favorable agreement.

It is often believed that the opacity effects on the line emission intensities in laboratory plasmas might be small enough to use diagnostics developed for optically thin plasmas if the size of the emitting region of the laboratory plasma was small or the densities were not extremely high. To illustrate the opacity effects on laboratory plasmas, we have plotted the temperature dependence on the line ratios in the optically thick case in Figs. 11–14 for a plasma of 10^{20} ions/cm^3 and radii of 50 and 500 μm, typical of a laser-produced plasma and an exploding wire plasma. In all ratios but the H(L_β) to He(L_δ), the transport of the radiation has a significant effect on the values that would be determined for the electron temperature. In fact, the error incurred by using optically thin calculations for these plasmas can be as much as 200–300 eV for the 500 μm plasma and 100–200 eV for the 50-μm plasma. Curiously enough, the ratios may also be useful in determining the size of the emitting region.

Looking more closely at the optically thick calculations plotted in Figs. 12–14, the results for the larger-radius plasma yield values for the line ratios which are larger at low temperatures and smaller at high temperatures than those predicted by the optically thin calculation. This is a reflection of the shift in abundances from the AlXII ion to the AlXIII ion as electron temperature increases. At 500 eV, the $1s^2$ level is more populated than the $1s$ level; consequently, the optical depths of the heliumlike Lyman lines are greater than those of the hydrogenlike Lyman lines, and the greater attenuation of line radiation from AlXII excited states is manifested in the enhancement of the line ratios. At 1600 eV, the opposite is true of the relative abundances of the $1s^2$ and $1s$ levels; therefore, the line ratios will be decreased somewhat compared to those calculated in the optically thin approximation.

D. Comparison with LTE model

Since the ionization-radiation model described here is characterized both by particle collisions and photon processes in an equilibrium mode, it was termed a collisional-radiative model. Another model frequently used to calculate the plasma atomic state is the LTE model.[10] The models differ in that the LTE assumption presupposes that a radiative process is negligible when compared to a competing collisional process. The CRE model, however, takes both processes into account, explicitly. An abundance curve, calculated using an LTE model, is shown in Fig. 3 (broken curves) for a plasma at 300 eV, alongside the CRE results. As would be expected, the higher ionization stages approach the LTE limiting values at higher densities; lithiumlike states attain their LTE values at an ion density of 2×10^{22} cm^{-3}, while this occurs for the heliumlike, hydrogenlike, and stripped ions at densities of 10^{23}, 3×10^{23}, and 6×10^{23} ions/cm^3, respectively.

Because of its simplicity, the LTE ionization model has had widespread applications in the plasma community for the purpose of diagnostics and effective charge determinations in laboratory plasmas. To test the validity of the application of the LTE model, simple expressions[11] have been offered to determine whether plasma conditions are within the constraints of the LTE regime. The basis of these expressions is the notion that a collisional rate depopulating a level must be a factor of 10 greater than a competing radiative rate from this level for the state population to be within 10% of its LTE value. We will attempt to show, here, that this can be too strict a density requirement.

If we consider the rates which couple the AlXIV ion to the AlXIII ground state, the competing processes are collisional (3-body) recombination and radiative (2-body) recombination. The collisional recombination rate coefficient is given by,[8] in cm^6/sec,

$$\beta = 8.05\times10^{-28}(g_l/2g_u)\,\zeta\chi^{-2}T_e^{-1} \tag{19}$$

while an approximate expression can be used for the radiative rate coefficient,[35] in cm^3/sec,

$$\alpha \cong 5.2\times10^{-14}Z\lambda\,(0.43+\tfrac{1}{2}\ln\lambda+0.469\lambda^{-1/3}), \tag{20}$$

while g is the statistical weight, ζ is the number of outer-shell electrons, χ is the ionization energy, Z is ion charge, $\lambda=\chi/T_e$, and u and l refer to upper and lower states. The ratio $\beta N_e/\alpha$ becomes equal to 10 at an electron density of about 1.7×10^{26} cm^{-3} yielding an ion density of about 6×10^{25} cm^{-3}. Hence, these two ground states should attain the population density ratio close to that predicted by the Saha equation for a plasma at 300 eV above an ion density of 6×10^{25} ions/cm^3. A similar calculation for the hydrogenlike and

heliumlike ground states yields an ion density of about 9×10^{25} cm^{-3} at 300 eV.

A similar estimate can be applied to excited states, where the collisional-deexcitation rate coefficient must exceed the largest competing radiative decay rate by about a factor of 10 for the upper and lower states to be in LTE with each other. If we consider the $1s$-$2p$ transition in AlXIII and employ the collisional-excitation rate coefficient from our distorted-wave calculation, the ion density required for these levels to be in LTE with respect to each other is around 1×10^{24} cm^{-3}. A similar calculation with the $1s^2$-$1s2p\,^1P$ transition indicates that an ion density of at least 1.5×10^{24} cm^{-3} is required for these two levels to equilibrate to their LTE values.

The values obtained from these simple expressions are noticeable higher than those predicted by the CRE model as seen in Fig. 3. It would appear that the use of the above expressions neglects the rather important effect of the interplay between the levels which lie in energy between the ground states. Since the density at which states equilibrate to their LTE values generally increases with energy separation, many close-lying levels will reach their LTE population ratios at much lower densities than the cases considered above which are typified by large energy differences. In an apparent "bootstrapping" process, the coupling between these levels and the ground states is enough to cause significant equilibration of the ground states toward LTE at densities significantly lower than those predicted by a simple test involving an isolated 2-level system. Hence, a collisional-radiative treatment with some excited-state structure included is necessary to accurately ascertain at what density and temperature a plasma can adequately be described by an LTE model.

Although the restrictions on the density required for LTE are seen to be eased somewhat by the results of this study with the CRE model, care must be taken when making theoretical predictions based on diagnostics from an LTE calculation. At densities where K-shell excited states have equilibrated to their LTE population ratios but the ground states have not, the absolute populations of the excited states (and consequently the radiation emission) will be incorrect, since they are determined relative to the still non-LTE ground-state densities.

It is well known that photoexcitation in an opaque plasma will force it toward a state of LTE at lower densities than would be predicted in the optically thin approximation. To illustrate, opacity effects were included in the calculation for a 100-μm, 300-eV plasma, and the fractional distributions plotted in Fig. 3 (dotted-dashed lines) also. Notice that the optically thick CRE results are always between the optically thin CRE and the LTE predictions, and that there is a substantial change in the populations in a direction closer to those for LTE over a density range of 10^{20}–10^{22} ions/cm^3. Notice also, however, that the plasma becomes collision dominated above 5×10^{22} ions/cm^3 and the CRE calculation with opacity effects included does not differ significantly from the CRE thin prediction of the density at which the plasma finally attains the LTE state.

IV. DISCUSSION

This work has investigated some of the fundamental aspects of line emission from a hot dense aluminum plasma. In particular, we have examined the radiation signature by modeling the plasma ion dynamics using a collisional-radiative model which includes opacity effects. Line ratios were calculated and then compared, in two cases, with older theoretical predictions, and contrasted with the result predicted when opacity effects are taken into account. We have shown that what may appear to be a well-behaved and understood diagnostic in an optically thin approximation may, in fact, be a rather complex double-valued function dependent on both plasma temperature and density when the optical depth of a photon through the plasma becomes large. An important result of this work which we would like to stress is not that these line ratios may become ineffective diagnostic tools when they are taken from a spectra emitted from an optically dense plasma. Rather, it now becomes apparent that a comprehensive treatment of the radiation diagnostics is required. Close agreement between a number of separate temperature or density diagnostics can resolve the dilemma of double valuedness. The comparison of parameters determined from line ratios and those obtained from other methods such as series merging,[36] Stark profiles,[37] or slope of the continuum can also be an effective technique. However, the entire spectrum must be analyzed in detail to properly make use of the plasma diagnostic techniques available.

The results of this model have also been compared with the LTE result and it has been seen that the plasma cannot be fully described by an LTE model until rather large densities have been obtained. Although, in an opaque plasma, excited states may approximate their LTE populations at a significantly lower density than in an optically thin plasma, due to optical pumping through reabsorption of photons, the ground states will still maintain populations between the LTE and coronal limits at this lower density, only slightly affected

by the opacities considered here. Thus, though the excited-state populations may be correctly determined relative to the next-higher ground-state density, line ratios calculated from lines which originate in excited states from different ionization stages will be in error since the ground states are not accurately given by their LTE-determined values. It is also worth noting that there is a disagreement between abundance curves quoted here and those shown in Ref. 9, which depicts highly overpopulated Al III and Al XI ions. This result appears unphysical in light of the previous discussion of electron shell configurations and their effect on the ionization dynamics. The lithium-like ion with an ionization potential of 442 eV should ionize easily to the closed-shell Al XII ion and should never constitute a major partial density fraction over a wide range of temperatures at an ion density of only 10^{22} cm^{-3} as is shown in Ref. 9. This is in agreement with work done previously by other authors[38,39] on aluminum as well as other materials of nearly the same atomic number. In addition, the study in Ref. 9 includes a graph showing that their CRE model is in agreement with the LTE result for the Al XIV population at an ion density of about 5×10^{22} cm^{-3}, a factor of 10 lower than in Fig. 3. It is our opinion that this disagreement is due to their collisional-ionization rate from Al XIII. An approximate form for the rate is given in Ref. 6, in cm^3/sec,

$$S \propto \zeta \chi^{-2} T_e^{1/2} e^{-\chi/kT_e}, \tag{21}$$

where ζ is the electron number in the outermost shell. This would predict a rate for Al XII which is about twice as large as that for Al XIII (ionization potentials are within 10% of each other). This is in disagreement with Fig. 5 of Ref. 9 which shows the Al XIII rate to be about two orders of magnitude greater than the Al XII rate at $T_e = 300$ eV. The Al XII collisional-ionization rate used in this study is in good agreement with the one quoted in Ref. 9, hence it is the questionably large Al XIII ionization rate which is the cause of their Al XIV population.

Some discussion of the approximations made in constructing this model is warranted in order to properly assess the significance of the analysis presented here. The equations governing the physics described above are solved numerically by a zero-dimension (single-zone) computer model; this allows only for treatment of plasmas which are homogeneous in temperature and density at the time of the radiation pulse. In addition, the rate equations are solved time-independently; hence, the assumption is made that the width of the radiation pulse is small compared to the hydrodynamic time scale of the plasma. The atomic level structure used was selected in order to describe the most important K-series emission lines, based on analysis of experimental spectra and the states contributing most significantly to its formation, either quantitatively or qualitatively (within the temperature range of interest of this work). Thus, we have retained some structure which is less important energetically, for diagnostic purposes. We have not included detailed structure in most of the L-shell ions, leaving that for later investigations. Finally, several atomic processes have been omitted such as multiphoton excitation, photoionization, and inner-shell collisions. The model retains the flexibility to include these processes in future work, but their contribution toward the determination of the level populations is considered of less importance in plasmas studied in this paper.

ACKNOWLEDGMENTS

The authors would like to thank Dr. J. Rogerson for his aluminum LTE calculations, Dr. V. Jacobs for calculating the dielectronic recombination rates, and Dr. P. C. Kepple and Dr. K. G. Whitney for helpful discussions and suggestions. One of us (D.D.) was supported by an NRC-NRL Resident Research Associateship. This work was supported in part by the Defense Nuclear Agency.

*Present address: Science Applications, Inc., McLean, Virginia.

[1]K. B. Mitchell, D. B. Van Hulsteyn, G. H. McCall, Ping Lee, and H. R. Griem, Phys. Rev. Lett. 42, 228 (1979).
[2]B. Yaacobi, D. Steel, E. Thorsos, A. Hauer, and B. Perry, Phys. Rev. Lett. 39, 1526 (1977).
[3]J. Mizui, N. Yamaguchi, T. Yamanaka, and C. Yamanaka, Phys. Rev. Lett. 39, 619 (1977).
[4]J. P. Apruzese, J. Davis, and K. G. Whitney, J. Appl. Phys. 47, 4433 (1976); 48, 667 (1977).
[5]A. L. Hoffman and E. A. Crawford, J. Appl. Phys. 49, 3219 (1978).
[6]R. K. Landshoff and J. D. Perez, Phys. Rev. A 13, 1619 (1976).
[7]D. Duston and J. J. Duderstadt, J. Appl. Phys. 49, 4388 (1978); Phys. Rev. A 18, 1707 (1978).
[8]J. Davis and K. G. Whitney, J. Appl. Phys. 45, 5294 (1974).
[9]D. Salzmann and A. Krumbein, J. Appl. Phys. 49, 3229 (1978).
[10]J. Richter, in *Plasma Diagnostics*, edited by W. Lochte-Holtgreven (North-Holland, Amsterdam, 1968).
[11]R. W. P. McWhirter, in *Plasma Diagnostic Techni-*

ques, edited by R. H. Huddlestone and S. L. Leonard (Academic, New York, 1965).
[12]D. G. Colombant, K. G. Whitney, D. A. Tidman, N. K. Winsor, and J. Davis, Phys. Fluids 18, 1687 (1975).
[13]D. Duston and J. Davis, NRL Memorandum Report No. 3846, 1978 (unpublished).
[14]M. J. Seaton, Proc. Phys. Soc. London 79, 1105 (1962).
[15]V. L. Jacobs, J. Davis, P. C. Kepple, and M. Blaha, Astrophys. J. 211, 605 (1977).
[16]W. J. Karzas and R. Latter, Astrophys. J. Suppl. Ser. 6, 167 (1961).
[17]V. L. Jacobs and J. Davis, Phys. Rev. A 18, 697 (1978).
[18]W. Wiese, M. Smith, and B. Miles, *Atomic Transition Probabilities* (U.S. GPO, Washington, D.C., 1969), Vol. II.
[19]L. A. Vainshtein, and I. I. Sobel'man, Lebedev Report No. 66 (1967); I. I. Sobel'man, *Introduction to the Theory of Atomic Spectra* (Pergamon, Oxford, 1972).
[20]J. Davis, P. C. Kepple, and M. Blaha, J. Quant. Spectrosc. Radiat. Transfer 16, 1043 (1976).
[21]George B. Field, Astrophys. J. 129, 551 (1959).
[22]D. G. Hummer, Astrophys. J. 140, 276 (1964).
[23]P. S. Julienne and J. Davis, NRL Memorandum Report No. 2556, 1973 (unpublished).
[24]A. G. Hearn, Proc. Phys. Soc. London 81, 648 (1963).
[25]P. G. Burkhalter, C. M. Dozier, and D. J. Nagel, Phys. Rev. A 15, 700 (1977).
[26]L. F. Chase, W. G. Jordan, J. D. Perez, J. G. Pronko, Appl. Phys. Lett. 30, 137 (1977).
[27]P. Burkhalter, J. Davis, J. Rauch, W. Clark, G. Dahlbacka, and R. Schneider, J. Appl. Phys. 50, 705 (1979).
[28]A. V. Vinogradov, I. Yu. Skobelev, and E. A. Yukov, Kvant. Elektron. (Moscow) 2, 1165 (1975) [Sov. J. Quantum Electron. 5, 630 (1975)].
[29]H. J. Kunge, A. H. Gabriel, and H. R. Griem, Phys. Rev. 165, 276 (1968).
[30]E. V. Aglitskii, V. A. Boiko, A. V. Vinogradov, and E. A. Yukov, Kvant. Elektron. (Moscow) 1, 579 (1974) [Sov. J. Quantum Electron. 4, 322 (1974)].
[31]C. D. Lin, W. R. Johnson, and A. Dalgarno, Phys. Rev. A 15, 154 (1977).
[32]A. H. Gabriel and C. Jordan, in *Case Studies in Atomic Collision Physics*, edited by E. W. McDaniel and M. H. McDowell (North-Holland, Amsterdam, 1972), Vol. 2.
[33]H. Van Regemorter, Astrophys. J. 136, 906 (1962).
[34]C. P. Bhalla, A. H. Gabriel, and L. P. Presnyakov, Mon. Not. R. Astron. Soc. 172, 359 (1975).
[35]M. J. Seaton, Mon. Not. R. Astron. Soc. 119, 81 (1959).
[36]J. Davis, NRL Memorandum Report No. 2655, 1973 (unpublished).
[37]H. R. Griem, M. Blaha, and P. C. Kepple, Phys. Rev. A 19, 2421 (1979).
[38]C. Jordan, Mon. Not. R. Astron. Soc. 142, 501 (1969).
[39]L. L. House, Astrophys. J. Suppl. Ser. 8, 307 (1964).